Available online at www.sciencedirect.com
SCIENCE DIRECT®
Coordination Chemistry Reviews 249 (2005) 161–177
COORDINATION CHEMISTRY REVIEWS
www.elsevier.com/locate/ccr

Review

Characterization of "spectroscopically quiet" metals in biology

James E. Penner-Hahn*

Department of Chemistry, Biophysics Research Division, University of Michigan, Ann Arbor, MI 48109-1055, USA

Received 1 January 2004; accepted 23 March 2004
Available online 2 November 2004

Contents

Abstract

The use of X-ray absorption spectroscopy (XAS) to characterize the local environment of "spectroscopically quiet" metals in metalloproteins is reviewed, with an emphasis on studies of Cu(I) and Zn(II). Both the advantages and the weaknesses of X-ray absorption are discussed, with examples taken from the recent literature.

Keywords: Spectroscopically quiet; X-ray absorption; Cu(I); Zn (II); EXAFS; XANES; XAS

1. Aims and scope of review

1.1. Definition of "spectroscopically quiet" metals

Over the last 40 years, there have been tremendous advances in our understanding of bioinorganic chemistry. Many of these can be traced, in one way or another, to spectroscopic studies of metalloprotein active sites. Particularly informative have been studies in the UV-Vis (absorption, CD, and MCD) and microwave (EPR, ESEEM, ENDOR, etc.) spectral regions. The importance of the UV-Vis and microwave regions rests, in part, on the fact that many metals have intense, spectroscopically unique signatures in these regions. Thus, the visible spectroscopy of heme proteins and the EPR spectroscopy of Cu

* Tel.: +1-734-764-7324; fax: +1-734-647-4865.
E-mail address: jeph@umich.edu (J.E. Penner-Hahn).

0010-8545/$ – see front matter © 2004 Elsevier B.V. All rights reserved.
doi:10.1016/j.ccr.2004.03.011

proteins were among the earliest bioinorganic investigations.

Unfortunately, metals with either filled or empty d-shells have almost no spectroscopic signature (i.e., are "spectroscopically silent") in both spectral regions. Of these metals, the most important biologically are Cu(I) and Zn(II) as trace elements and Na(I), K(I), Mg(II) and Ca(II) as more abundant elements. For such metals, synchrotron spectroscopy, in particular X-ray absorption spectroscopy (XAS), may be the only method outside of crystallography for obtaining insight into the metal-site structure. These essential metals, together with important toxins such as Cd, Hg, and Pb, and important therapeutic reagents such as Ga or Au, make up the "spectroscopically quiet" metals (quiet, rather than silent, since they are readily accessible using core-level XAS). This review is intended to provide an overview of the use of X-ray absorption to characterize the roles of spectroscopically quiet metals in biology. The emphasis is placed on Cu(I) and Zn(II) rather than Na(I), K(I), Mg(II), or Ca(II), as the former tend to form tightly-bound complexes with proteins and thus to give data that is more straightforward to interpret. Rather than an exhaustive description of all of the examples of Cu(I) and Zn(II) spectroscopic studies, an effort has been made to select examples that illustrate key features of such studies.

Another group of elements that are not accessible using conventional spectroscopies are most of the ligand elements. Recent work has shown that X-ray spectroscopy is equally useful for characterizing the local environment of ligands, especially those containing S or Cl [1–3]. This has been reviewed recently, including a contribution in the present volume [4,5], and thus is not included in the present review.

1.2. Alternatives to XAS

In addition to XAS, there are a few other spectroscopic probes that can be used to examine spectroscopically quiet metals. Mercury (^{199}Hg), cadmium (^{113}Cd), and silver (^{109}Ag) can be studied directly by NMR and, in addition, show ligand-to-metal charge transfer transitions that can be used to characterize metal–thiolate interactions [6–9]. Recently, time-differential perturbed angular correlation has been developed as a probe for investigating the local environment of Cd and Hg in biological systems [10]. This utilizes the time-correlation in the γ-ray emission from radioactive nuclei (^{111}Cd and ^{199m}Hg) to characterize the nuclear quadrupole interactions at the metal site. Unfortunately, none of these approaches are useful for studies of Zn(II) or Cu(I). Very recently, there has been exciting progress in using solid-state NMR to characterize Zn sites [11–13]. However, solid-state NMR is not, at least yet, generally applicable as a tool for understanding biological Zn environments.

Often, it is possible to substitute an active site Zn or Cu with a spectroscopically accessible probe. Cobalt, which has both EPR and UV-Vis bands, has been used as a surrogate for zinc for many years [14,15], and often can be substituted with little or no loss of reactivity. Similarly Cd(II) will often substitute for Zn(II) and Ag(I) for Cu(I) [16–19]. Although it is not necessarily the case that any of these substitutions are isostructural [20,21], they can nevertheless be very useful for obtaining some information about Cu or Zn structure. Since the present volume is focused on the applications of synchrotron radiation, ancillary techniques will be discussed only in those cases that they provide an essential complement to information available from XAS.

2. X-ray absorption spectroscopy

2.1. Physical principles of XAS

XAS is one of the premier tools for investigating the local structural environment of metal ions. It can be divided into X-ray absorption near edge structure (XANES), which provides information primarily about geometry and oxidation state, and extended X-ray absorption fine structure (EXAFS), which provides information about metal site ligation. In the present context, the three key attractions of XAS are that it is element specific, that it is always detectable, and that it can be used to study dilute non-crystalline samples. The last of these has been particularly important in the past, when protein crystal structures were relatively rare and XAS was the only way to obtain structural information for many metal sites. With the initiation of numerous structural genomics efforts worldwide, protein crystal structures are becoming less rare. One of the goals of the present review is to emphasize that even in the era of structural genomics, XAS has an important role to play in developing a complete description of metalloprotein metal sites (see Section 5).

XAS has been available as a useful structural probe for nearly 30 years, and over this time a variety of excellent reviews and monographs have been written describing the method [22–30]. The following provides a brief review of this background information.

X-rays have sufficient energy to eject one or more core electrons from an atom. Each core electron has a well-defined binding energy, and when the energy of the incident X-ray is scanned across one of these energies, there is an abrupt increase in the absorption coefficient. This is the so-called "absorption edge" of the element. The remainder of this review is concerned almost exclusively with measurements made at the K-edge (1 s initial state). For first row transition metals, the K-edge energy is in the hard X-ray region (5–10 keV, or ca. 2–1 Å). The absorption coefficient near an edge typically shows fine structure that is divided, somewhat arbitrarily, into XANES and EXAFS regions, with the former referring to structure within ca. 50 eV of the edge and the latter to structure at higher energy (see Fig. 1).

The physical basis of both EXAFS and XANES is the scattering of the X-ray excited photoelectron by the

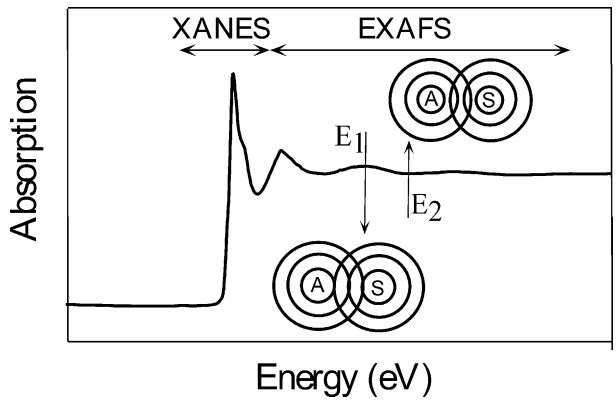

Fig. 1. Schematic illustration of an X-ray absorption spectrum at the Zn K-edge. The insets show the interference phenomena that give rise to the modulations in absorption cross-section (see text). In the insets, *A* and *S* refer to the absorbing and scattering atoms, respectively. The concentric circles around *A* and *S* represent the maxima in the photoelectron wave that describes the propagation of the X-ray excited photoelectron. Constructive interference between the outgoing and back-scattered waves (E_1) give a local maximum in absorption; destructive interference (E_2) gives a local minimum.

surrounding atoms, as illustrated schematically in the insets to Fig. 1. As the X-ray energy increases, the kinetic energy of the photoelectron increases and the photoelectron wavelength decreases. This results in alternating destructive and constructive interference as the energy increases (energies $E1$ and E_2 in Fig. 1). EXAFS can thus be thought of as a spectroscopically-detected electron scattering experiment. As this description suggests, EXAFS has both the advantages of electron scattering (sensitivity to local structural information) and the disadvantages (the information of interest is encoded over the entire scattering region, rather than localized in a single spectral peak).

If X-ray energy is converted to photoelectron wavevector k (k is the inverse photoelectron wavelength, $k = \sqrt{2m_e(E - E_0)/\hbar^2}$), the EXAFS for a single absorber–scatterer pair takes a particularly simple sinusoidal form (Eq. (1)):

$$\chi_i(k) = \frac{N_s A_s(k)}{R_{as}^2} \exp(-2k^2\sigma_{as}^2) \sin(2kR_{as} + \phi_{as}(k)) \qquad (1)$$

In Eq. (1), χ_i is the fractional modulation in X-ray absorption cross-section due to the scattering from the ith absorber–scatterer pair. The structurally interesting parameters are N_s, the number of scattering atoms, R_{as}, the absorber–scatterer distance, and σ_{as}^2, the mean-square disorder in absorber–scatterer distance (often referred to as the Debye–Waller factor). For more complex structures, having more than one absorber–scatterer distance, the EXAFS is given by the sum of the individual interactions (Eq. (2)):

$$\chi(k) = \sum_{i=1}^{n} \chi_i(k) \qquad (2)$$

In Eq. (2), the sum should, in principle, be taken over all absorber–scatterer pathways. In practice, however, even a relatively simple structure may have tens to hundreds of relevant pathways. To simplify the analysis, these are typically grouped into "shells", where a shell represents the scattering from several chemically similar atoms, all at approximately the same distance from the absorber.

In order to use Eqs. (1) and (2) for structural analysis, one needs to know the parameters $A_s(k)$ and $\phi_{as}(k)$. These represent, respectively, the energy dependence of the photoelectron scattering, and the phase shift that the photoelectron wave undergoes when passing through the potential of the absorbing and scattering atoms. These amplitude and phase parameters contain the information necessary to identify the scattering atom. Thus, for example, sulfur and oxygen introduce phase shifts, $\phi_{as}(k)$, that differ by approximately π. Unfortunately, both $A_s(k)$ and $\phi_{as}(k)$ depend only weakly on scatterer identity, making it difficult to identify the scatterer with precision. In the biological context, this typically means that O and N, or S and Cl, cannot be distinguished, while N and S can, at least in principle be distinguished (although see Section 3.1). While scatterers such as C or F cannot easily be distinguished from O and N, this seldom causes any ambiguity.

Although Eq. (2) provides a complete description of the EXAFS oscillations, it is not a particularly convenient form for visualizing the information content of an EXAFS spectrum. As with NMR spectroscopy, Fourier transformation can be used to decompose an oscillatory signal into its different constituent frequencies, going from k (in $Å^{-1}$) and R (in Å), and giving a pseudo-radial distribution function. As a consequence of the phase shift $\phi_{as}(k)$, the apparent distances in the Fourier transform (FT) are shifted by about −0.5 Å.

The FT alone does not give reliable structural results: the FT can show only a single peak, even when the sample contains multiple shells, and, even more misleadingly, interference between two different peaks in the FT may give rise to a spurious third peak [29]. In order to obtain reliable structural parameters, it is necessary to use curve-fitting to model the data. Quantitative analysis of EXAFS data involves fitting the experimental data to Eq. (2) (or its equivalent), using amplitude and phases parameters that are derived either from ab initio calculations or from model compounds of known structure. In recent years, the available theoretical methods for quickly and accurately calculating these parameters have improved dramatically. Ab initio calculations are now relatively straightforward [31–33], although careful comparison with model compounds remains important for proper calibration of the calculated parameters [34].

EXAFS can be analyzed quantitatively to determine R with an accuracy of ca. 0.02 Å (and a precision that can be as good as 0.004 Å [35]) and N with an accuracy of ca. 25%. The low accuracy of N results, in part, from the fact that N and σ^2 are highly correlated, particularly for data measured over a limited range of k space.

2.2. A few words of caution

Despite the obvious strengths of XAS as a structural probe, there are several limitations that need to be considered. While these affect all XAS studies, they can be particularly problematic for studies of the spectroscopically quiet metals, since in these cases there usually is no parallel spectroscopic probe that can be used to validate conclusions drawn from XAS spectroscopy.

Perhaps the most obvious limitation of XAS is that only the *average* structure can be determined. If the metal of interest is present in multiple environments, or if adventitious metal is bound, the structure determined by XAS will not represent the structure of the active site. This can be particularly important for studies of Zn, since Zn is ubiquitous, and is often found to bind adventitiously to proteins. In some cases, the extra metal may be weakly bound at an inhibitory site, as in recent study of *N*-acetylglucosamine deacetylase [36], and can be removed with chelators. In other cases, it may be necessary to completely remove all of the metal from the protein before adding back one equivalent of the metal of interest in order to obtain a homogeneous sample [37]. Particularly problematic are proteins that are purified using a poly-histidine tag. Since histidine has a high affinity for metals, His-tagged proteins are especially likely to bind adventitious zinc. If the active site is not fully occupied, it may be impossible to tell from stoichiometry alone that adventitious metal is bound. This may be responsible for the recent finding that the Zn in coenzyme M methyltransferase is bound to only a single thiolate [38], when closely related proteins appear to have two thiolate ligands.

A second difficulty is that EXAFS spectra are typically measured over only a limited k range. This has two consequences. One is to limit the bond-length resolution. Two scattering shells can only be resolved if they differ sufficiently in frequency to cause a detectable change in the EXAFS amplitude. For noise-free data, two shells of the same scatterer should become resolvable when the difference in their distances, δR, is large enough to cause a "beat" in the EXAFS amplitude. This occurs for $\delta R \geq \pi/2k_{max}$, where k_{max} is the maximum value of k for which a signal can be measured. If two shells are separated by less than δR, the EXAFS from these two shells will be indistinguishable from the EXAFS for a single disordered shell at the average of the two distances. Typical values of k_{max} range from 12 to 20 $Å^{-1}$, giving $\delta R = 0.08$–0.13 Å. In reality, the effective δR is somewhat larger, since noise in the data, particularly at high k, limits the ability of EXAFS to resolve bond length differences. This is illustrated, for example, in Fig. 4 of [29].

A third limitation is due to the fact that EXAFS spectra contain only a limited number of independent degrees of freedom. If the minimum separation that can be detected is δR (above), and the useful data covers an R range of ΔR, then the number of independent data points is $\Delta R/\delta R$. Since the useful k range does not extend to $k = 0\,Å^{-1}$, a better expression for the number of independent data points, N_{idp}, is $2\Delta k \Delta R/\pi$ [39]. For $\Delta R = 2$ Å (e.g., useful information for R = 1–3 Å) and $\Delta k = 12\,Å^{-1}$ (k = 2–14 $Å^{-1}$), this gives approximately 16 degrees of freedom in a typical data set. More involved derivations give slightly different N_{idp} values [40], but do not alter the essential result that the number of available degrees of freedom is severely limited. This creates the potential for errors if one does not keep careful track of variable parameters [34,41].

If one used crystallographic criteria that the data/parameter ratio should not be less than 5, a typical EXAFS analysis would be limited to two or three variable parameters (i.e., to a single shell). A similar difficulty with parameter under-determination occurs in protein crystallography. In that case, the solution has been to include structural constraints, such as the known bond lengths and angles within amino acids, as part of the refinement. This approach has been used to good effect in refinements of the EXAFS scattering by rigid imidazole groups as a ligand in bioinorganic complexes [33,42,43]. By adding constraints, it is possible to increase the number of shells that are used to describe the EXAFS without increasing (too much) the number of freely variable parameters. It is important to keep in mind, however, that constraints are only as good as the model upon which they are based. Erroneous assumptions in building the constraints may give fits that are mathematically very good, but chemically meaningless.

For seriously under-determined systems, even constrained refinements may give a data:parameter ratio that is not much larger than 1 (or even smaller than 1 in some instances [44]). In such cases, it is better to think of the EXAFS simulation as showing that a particular structural model is *consistent with* the data, rather than showing that it is *required by* the data. Although genuine curve fitting and data simulation are both legitimate approaches to interpreting EXAFS spectra, they do not provide the same information. Curve fitting, when done properly, describes the structural parameters that are required by the data. In contrast, a successful simulation gives only *a* model of the data, not necessarily the correct model.

It is important to note that the limitations on N_{idp} are a general property of EXAFS, and not specific to the details of the data analysis (e.g., k-space versus R-space fitting, k-weighting, etc.). The number of measured data points is usually much larger (often by 10–20-fold) than N_{idp}. This can be important for analyses using statistical tests to judge whether an added shell is required by the data [39,45], since use of N in place of N_{idp} [46] will greatly overestimate the significance of an added shell. Even with the correct N_{idp}, several authors have noted [34,41] the need to exercise caution with statistical tests in order to avoid either false positives (inclusion of shells that are not actually present) or false negatives (exclusion of shells that are present).

2.3. Multiple scattering

In the physical model presented above, the X-ray excited photoelectron travels from the absorbing atom to the scattering atom and back. However, far more complex scattering pathways are also possible, known collectively as multiple scattering. As a practical matter, the most important consequence of multiple scattering in biological EXAFS has been that the rigid imidazole ring of a histidine ligand gives rise to diagnostic peaks that can be used to identify the presence of histidine ligands to a metal [33,43,47–49].

Multiple scattering depends on the relative positions of three or more atoms, i.e., on the distances and angles between the atoms. This means that multiple scattering can, at least in principle, provide information about the three dimensional structure around the absorbing site. Many authors, including a contribution in this volume [50], have explored the use of multiple scattering for determining three-dimensional structure. Although this is potentially very important for spectroscopically quiet metals, where there is often no other source of geometric information, detailed discussion of multiple scattering is beyond the scope of the present review. It is worth noting, however, that multiple scattering does not eliminate the problem of data under-determination, and can in fact exacerbate this problem. The difficulty arises because multiple scattering typically occurs only for outer shell atoms (i.e., for atoms at greater than ca. 3 Å from the absorber, although an exception to this in the case of PcoC is discussed is Section 3.3). Consequently, the *R* range over which multiple scattering is important tends to be relatively small and the number of independent data points that are sensitive to multiple scattering is likewise small. Since multiple scattering depends on three-dimensional structure (as opposed to the two-dimensional *radial* structure that defines single scattering) there are potentially even more parameters to refine, giving even worse under-determination. As with single scattering, this can be dealt with by a variety of simplifying assumptions.

3. EXAFS studies of proteins

3.1. Determination of ligation

For biological metal sites, the possible ligands are, under most conditions, limited to sulfur (thiolate, thioether, or sulfide), oxygen (water, hydroxide, oxo, phenolate, or carboxylate) and nitrogen (imidazole). Most descriptions of EXAFS, including the one given above, indicate that it is possible to distinguish between ligands that differ by one row in the periodic table and thus that it should be possible to distinguish S from N or O ligands. While it is true that S and N/O scatterers give rise to readily distinguishable EXAFS signals in monoligated systems, it can be quite difficult to distinguish between these in mixed ligand systems. The origin of this difficulty can best be appreciated by comparing the Zn–S and Zn–N EXAFS signals (Fig. 2). The Zn–S EXAFS signal is nearly twice as large as the Zn–N signal and, perhaps more importantly, the two signals are out of phase over much of the useful data range, resulting in destructive interference. Destructive interference makes it difficult to distinguish, for example, between ZnS_2N_2 and ZnS_3N sites.

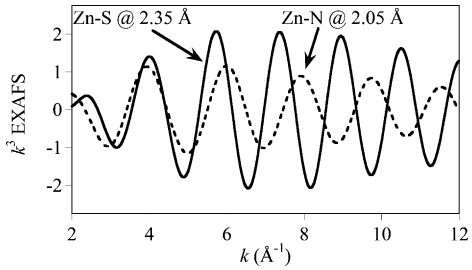

Fig. 2. Comparison of the EXAFS signals expected for Zn–S (solid line) and Zn–N (dashed line) scattering. Two ligands were assumed in the calculations, and chemically reasonable bond lengths were chosen. The Zn–S and Zn–N signals are out of phase for much of the usable data range.

These facts mean that the Fourier transform of a mixed ligand (S + N) site rarely shows resolvable peaks for Zn–S and Zn–N scattering [51]. Even with quantitative curve fitting, which is more reliable than Fourier transform comparison [30], distinguishing between various possible S + N ligation mixtures can be ambiguous. Although some simulations of S + N scattering give a detectable "beat" in EXAFS amplitude for mixed ligand systems [52], this is only seen for unrealistically short Zn–N distances of ca. 1.94 Å. With more realistic Zn–N distances of ca. 2.05 Å, there is often no clear evidence for mixed ligation. The difficulty is that it is *always* possible to fit an EXAFS signal as a mixture of S and N scatterers [51]. In particular, a fit using S + N is always better than a fit using S alone, regardless of whether the site has mixed S + N ligation or exclusively S ligation. This is due to the fact that two shell (S + N) fits have twice as many parameters as one shell (S only) fits. Unless the number of variable parameters is carefully controlled, it is very difficult to reliably define the Zn ligation.

One solution is to fit Zn EXAFS with a variable mixture of S + N ligation, leaving the total coordination number fixed [51]. The total coordination number can be constrained based on the observed bond length, since the average Zn–ligand bond length increases by ca. 0.1 Å on going from four- to five-coordinate, and on going from five- to six-coordinate. If the percent improvement in the fit, P_i, is defined as the improvement in the S + N fit relative to the improvement that would be seen simply by adding a second shell of scatterers, a plot of P_i versus %*S* shows characteristic behavior that can be used to distinguish between ZnS_2N_2, ZNS_3N, and ZnS_4 sites [34,53]. This is illustrated for a series of $Zn(SR)_n(Imid)_{4-n}^{2-n}$ models in Fig. 3.

The approach above is simply one of many ways in which the number of variable parameters can be constrained. Whatever approach is used, it is important to check that the

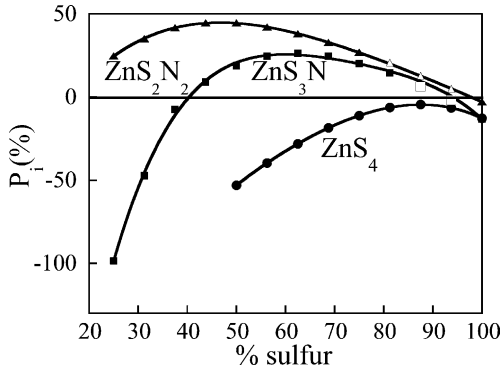

Fig. 3. Percent improvement (P_i) in fit quality as a function of the percentage of Zn–S scattering that was used in the fit [34]. Curves are shown for crystallographically characterized inorganic $Zn(SR)_4$ (circles), $Zn(SR)_3(imid)$ (squares) and $Zn(SR)_2(imid)_2$ (triangles) models. The different Zn sites give characteristic P_i curves that can be used to distinguish between different ligations. Note that even for the authentic ZnS_4 site, there is an improvement in P_i, i.e. the fit is better, when a nitrogen shell is added. Redrawn from data in [34].

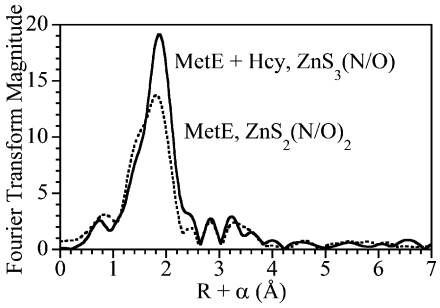

Fig. 4. Fourier transform of the EXAFS spectra for cobalamin-independent (MetE) methionine synthase. Native enzyme (dashed line), and MetE with substrate (homocysteine) added (solid line) [56]. The increase in Fourier transform amplitude reflects the change from N/O ligation to S ligation when Hcy binds. Redrawn from data in [56].

resulting structural parameters are physically reasonable. Thus, typical values of the Debye–Waller factor, σ^2, for crystallographically characterized model compounds range from 2×10^{-3} to 4×10^{-3} Å^2 [34]. If the apparent coordination number is too high, then the fitting algorithm can increase σ^2 in order to bring the overall EXAFS amplitude back to the experimental value. Similarly, when coordination number is too low, the fitted σ^2 is lower than expected. Thus, σ^2 values that differ significantly from the "normal" values may indicate a problem with the model.

One of the more intriguing observations from model studies was the fact that changing E_0 by a little as 5 eV can effectively convert a S scatterer into a N/O scatterer (or vice versa) [34]. This happens because the ability to distinguish between S and N/O, particularly in light of destructive interference (Fig. 2), is due to the phase difference between S and N/O scattering. Changes in E_0 change the apparent phase of an EXAFS oscillation, and thus interfere with the ability to distinguish between scatterers. In some EXAFS studies, E_0 is not only a freely variable parameter, but is even allowed to vary between scatterers. Fits in which there is significantly variation in E_0 (>2–3 eV), should be regarded with skepticism.

Methionine synthase provides an example of how EXAFS can be used to characterize the active site of a spectroscopically quiet protein. Methionine synthase catalyzes the transfer of a methyl group from tetrahydrofolate to homocysteine, a critical reaction in methionine biosynthesis [54]. This is a challenging reaction, since it requires nucleophilic displacement of a methyl group from methyltetrahydrofolate. Although thiolate is a potent nucleophile, thiol, the form that is present at physiological pH, is a very weak nucleophile. In some enzymes, methionine synthase methyl transfer is facilitated by the presence of a cobalamin group that forms a reactive methyl-cobalamin. However, there is also a cobalamin *independent* methionine synthase (MetE). Since MetE lacks the cobalamin co-factor, it must have some other method of activating the nucleophile [55].

The MetE protein was found to bind one equivalent of Zn [56], suggesting that Zn might play a role in catalysis. However, it was also possible that the Zn could be playing a purely structural role, promoting folding of the protein into a catalytically active form. The Fourier transforms of the EXAFS spectra for MetE and for MetE + homocysteine (Hcy) (Fig. 4) showed unambiguously that the Zn structure was affected by substrate binding. There is an increase in the height of the Fourier transform and a sharpening of the main peak, thus providing direct evidence that the substrate perturbs the Zn site and suggesting a catalytic role for the Zn [56].

Only a single peak is seen in the Fourier transform, although there is a poorly resolved shoulder on the low-*R* side of the main peak for the native protein, typical of those seen for ZnS_2N_2 sites. Consistent with this, the EXAFS data for the native protein was best modeled by two sulfurs at 2.31 Å and two oxygen/nitrogen ligands at 2.04 Å while the Hcy-bound protein was best fit with three sulfur ligands at 2.33 Å and one O/N ligand at 2.07 Å. This small increase in Zn–S distance is typical of those seen with an increase in the number of anionic ligands, as would be expected if a neutral O/N ligand were replaced by a thiolate. The EXAFS data provided the first direct evidence that the zinc site is intimately involved in catalysis, and not just playing a structural role. The increase in the number of sulfur ligands is consistent with the homocysteine sulfur binding directly to Zn.

Although EXAFS can identify the kind of ligands to the Zn, one of the weaknesses of EXAFS is that it is not sensitive to the precise identity of the ligands. Based on sequence comparison of 14 known MetE genes, there are two regions of conserved sequence: HXC at residues 641–643 and PDCG at residues 724–727 [57]. Based on the EXAFS evidence for $ZnS_2(O/N)_2$ ligation, it seemed likely that two of the Zn ligands were Cys643 and Cys726, although from EXAFS alone, it was possible that one or both of the apparent

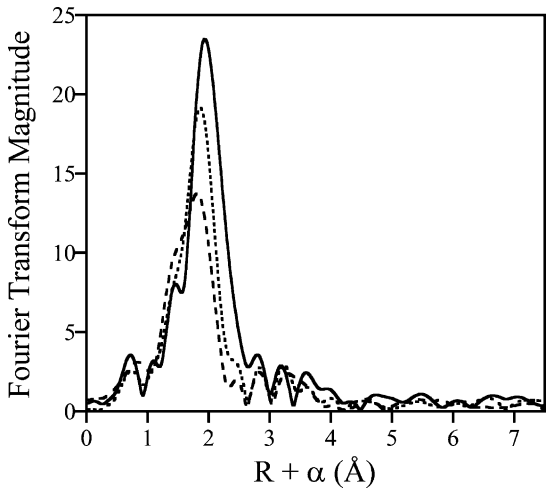

Fig. 5. Fourier transforms of the Zn EXAFS data for methionine synthases, showing the effect of different substrates on the Zn structure. Dashed line: native protein; dotted-line: enzyme + Hcy; solid line: enzyme + Se-Hcy. Redrawn from data in [59].

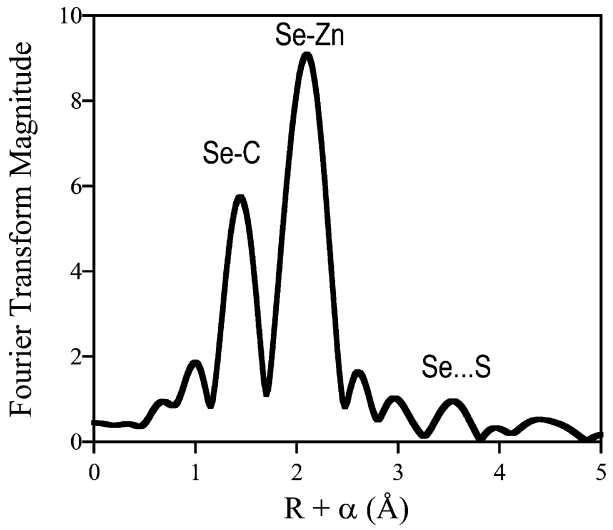

Fig. 6. Fourier transforms of the Se EXAFS data for Se-Hcy bound to MetE. Redrawn from data in [59].

S ligands was actually a Cl, or that a different, unconserved cysteine was one of the Zn ligands. Mutation of either conserved cysteine to alanine gave insoluble protein, suggesting the protein did not fold properly, while mutation to serine gave soluble protein with less than 0.3% of the activity of the native protein. These observations provided circumstantial evidence that Cys643 and Cys726 were indeed Zn ligands, although loss of activity in a mutant does not necessarily mean that the mutated amino acid is a ligand [58].

Positive identification of the Zn ligands came from EXAFS measurements [57] showing that both of the Cys → Ser mutants show perturbations in the EXAFS consistent with replacement of a cysteine sulfur by a low-*Z* ligand, presumably either a serine oxygen, or, perhaps more reasonably, a water molecule. Importantly, addition of Hcy to either mutant protein gave changes consistent with addition of a new S ligand, analogous to the behavior seen for the native enzyme, thus confirming that the Zn is bound at the same site in the mutants. Taken together, these data provide definitive evidence that Cys643 and Cys726 are Zn ligands.

The experiments described above are consistent with the Hcy sulfur binding to the Zn. However, they could not rule out the possibility that Hcy causes a change in the Zn ligation, but does not bind directly to the Zn. There are five other cysteines in MetE, thus it is possible, if unlikely, that the change in ligation illustrated by Fig. 4 is due to a conformational change such that a third endogenous cysteine binds to Zn.

To resolve this ambiguity, EXAFS data were measured for samples with homocysteine replaced by selenohomocysteine (Se-Hcy). Selenium is significantly heavier than the S in Hcy, and thus Se-Hcy has readily distinguishable scattering properties relative to Hcy. Since Se-Hcy reacts analogously to Hcy [59], EXAFS measurements provide direct insight into the Zn–S interaction. These data [59], shown in Fig. 5, are analogous to those seen using Hcy, although the increase in the Fourier transform amplitude is larger than the increase seen when Hcy binds. This is consistent with replacement of a Zn–O/N ligand by a Zn–Se ligand rather than by a Zn–S ligand. Quantitative fitting confirmed that the spectra could only be modeled by including Zn–(N/O), Zn–S, and Zn–Se interactions. The Zn–S and Zn–(N/O) shells gave distances similar to those found before, although these were somewhat less well defined due to interference from the strong Zn–Se signal and the increase in variable parameters. In contrast, the Zn–Se interaction was extremely well defined, with a single Zn–Se shell at 2.43 Å. These data provided direct evidence that the Se from Se-Hcy, and consequently the thiolate sulfur from Hcy, binds directly to the Zn.

The use of SeHcy allowed measurement of Se EXAFS in addition to Zn EXAFS. As expected, the EXAFS (Fig. 6) is dominated by Se–C and Se–Zn scattering, the Se–Zn distance was identical, to better than 0.01 Å, to the Zn–Se distance found in the Zn EXAFS, confirming the accuracy of the fitting. In addition, the Se EXAFS showed evidence for Se · · · S EXAFS (the weak outer shell feature in Fig. 6). Although this feature is small, it could only be modeled by including as Se–S shell. From the combined Zn–S, Zn–Se, and Se–S distances, it was possible to determine the average Se–Zn–S angle to be $104 \pm 3^{\circ}$. This is slightly smaller than that expected for a perfect tetrahedral geometry, perhaps reflecting a slight distortion in the site.

3.2. Determination of coordination number

In the data analysis protocol described in Section 3.1, the total coordination number of the zinc was held fixed at 4. While this is by far the most common coordination number for Zn(II), there are some examples of five- and six-coordinate sites. For Cu(I), coordination number is much

more variable, with numerous examples of two-, three-, and four-coordinate sites. In principle, it should be possible to distinguish between these possibilities using the EXAFS amplitude. In reality, most estimates of the uncertainty in EXAFS coordination numbers are about ±20% or 25%. This is sufficiently large that it is often impossible to distinguish between possible coordination numbers using EXAFS fits. In part, this uncertainty results from the correlation between N and σ^2 (see Eq. (1)), which both affect the observed EXAFS amplitude. This correlation can, in principle, be broken by careful experimental calibration of physically reasonable Debye–Waller factors (see Section 3.1) and by measuring data to higher k range, thereby enhancing the differences in the functional forms of N and σ^2. However, an added complication is that the EXAFS amplitude factors ($A_s(k)$ in Eq. (1)) are difficult to determine to better than approximately 10%, even with careful empirical calibration. As a consequence, even when uncertainties due to N and σ^2 are minimized, it remains difficult to obtain an unambiguous determination of coordination number from fits of the EXAFS.

Fortunately, EXAFS bond lengths can be used as a surrogate for coordination number. For a given ligand type, the average metal–ligand bond length increases as the coordination number increases. This correlation, which can be systematized as the so-called bond-valence-sum (Eq. (3)), has been used for many years by the geological community to characterize dopant ions in mineral crystals [60–62]:

$$S = \sum_i \exp(-0.37(R - R_0)) \tag{3}$$

In Eq. (3), R_0 is a constant characteristic of each metal–ligand pair and the sum is taken over all nearest-neighbors to the metal. The bond-valence-sum (S) is found to be equal to the formal valence of the metal, and this has been used to good effect in a number of studies of bioinorganic systems [63,64].

One of the main attractions of bond-valences-sums is that they rely on bond length, which can be determined with much greater accuracy than can coordination number. In Section 3.1, bond-valence-sums were used to confirm that the Zn sites were four-coordinate; in all cases the observed bond lengths were significantly shorter than would have been seen for a five-coordinate site.

The use of bond-length to determine coordination number has also been used extensively in studies of Cu(I) sites. If a Cu(I) protein contains a mixture of digonal and trigonal Cu–thiolate sites, the average bond length seen by EXAFS, R_{av}, will be the weighted average of the bond-lengths for the digonal and trigonal sites, R_d and R_t as in Eq. (4) [65]:

$$R_{av} = \frac{2x_d R_d + 3x_t R_t}{2x_d + 3x_t} \tag{4}$$

In Eq. (4), x_d and x_t are the mole fraction of digonal and trigonal Cu, respectively, and R_d and R_t were found from a study of Cu cluster models to be 2.16 and 2.28 Å, respectively. Given the observed Cu–S distance of 2.242 Å in *S. cerevisiae* metallothionein [65], Eq. (4) suggests that yeast metallothionein contains 30–40% digonal Cu(I) and 60–70% trigonal Cu(I). Although the biological relevance of digonal Cu(I) in metallothionein has been questioned (there are indications that digonal Cu(I) may be present only at higher metal:protein ratios [66,67]), the fact remains that Eq. (4), and analogous equations for other metals, can be very useful for determining coordination numbers using EXAFS.

3.3. Determination of geometry

EXAFS is most sensitive to radial structure, and gains sensitivity to three-dimensional geometry only through multiple scattering. Multiple-scattering is generally very weak for scattering angles of less than ca. 150°. This means that while multiple-scattering can be extremely useful for analysis of ligand geometry (e.g., in distinguishing between linear and bent nitrosyl ligands), EXAFS is relatively insensitive to the geometry of the metal site. The two notable exceptions to this are systems in which two or more absorption edges can be measured and systems that show significant first-shell multiple scattering. One illustration of the value of multiple edges is the use of Se and Zn edges in methionine synthase (Section 3.1). Another is the use of Cu and Se edges to characterize the structure of the binuclear CuA site in cytochrome ba3 [68]. In principle, this approach could also be used with sulfur EXAFS, although in practice this is complicated by the presence of multiple sulfur atoms in most proteins.

The ability of multiple scattering to determine geometry is based on its strong angular dependence. The intensity of multiple scattering increases dramatically as the scattering angle approaches 180°, with as much as a 10-fold enhancement in amplitude for linear systems [28]. Typically, intense multiple-scattering is seen for ligands such as cyanide or carbon monoxide, but can also be seen for first-shell scatterers. In this case, the scattering pathway is absorber → scatterer-1 → absorber → scatterer-2 → absorber. For first-shell scatterers, this is only of practical importance for near linear geometries (i.e., digonal sites, square-planar sites and octahedral sites) and is most important for heavy scatterers (e.g., sulfur). This phenomenon was used to show that the Cu-regulatory protein CueR contains a linear Cu–S_2 site [69]. The Cu–S distance of 2.14 Å indicated that the Cu site was two-coordinate (see Section 3.2), but could not distinguish between a linear site and a bent site. The latter would be expected if there was a weak interaction with a third ligand, that was too weakly bonded to perturb the Cu–S distance, but was still strongly enough interacting to give a bent S–Cu–S geometry.

The Fourier transform of the CueR EXAFS (Fig. 7) is dominated by an intense Cu–S nearest neighbor peak, but also contains two weaker outer-shell peaks. The first of these was attributed to Cu–C single scattering from the cysteine while the latter could only be modeled as Cu → S → Cu → S → Cu multiple scattering. The apparent Cu–S distance in the multiple-scattering pathway was ex-

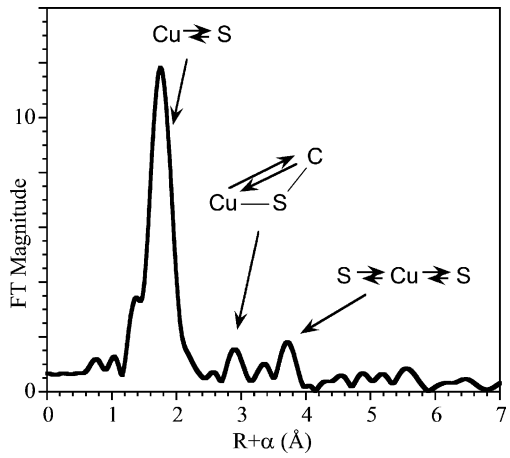

Fig. 7. Fourier transform of CueR EXAFS showing assignment of the major peaks in terms of Cu–S and Cu–C single scattering, and first-shell Cu–S multiple-scattering. The latter is only observed for linear complexes. Redrawn from data in [69].

actly twice the first-shell Cu–S distance, consistent with the multiple scattering interpretation of this peak. Based on the calculated angular dependence of the multiple-scattering, the S–Cu–S angle was shown to be greater than 175°. A smaller angle (i.e., a bent CuS_2 site) was unable to reproduce either the amplitude or the apparent distance of the first-shell multiple-scattering peak.

3.4. Determination of metal-site nuclearity

Many proteins bind more than one metal atom. Since EXAFS is sensitive to scatterers within ca. 3–4 Å of the absorbing atom, and since heavy atoms such as metals often give rise to detectable outer shell scattering, EXAFS should be able to tell whether the metals in a protein are bound together in a multinuclear cluster or are bound at separate sites. This has been used to demonstrate the presence of poly-copper clusters in, for example, the metallochaperone Cox17 [70] or the copper-regulated transcription factors Ace1 and Mac1 [71]. In each case, there was a clear outer-shell interaction attributed to a Cu–Cu distance of 2.7–2.9 Å. Due to the presence of multiple Cu ions, it was not possible to determine the precise geometry of the cluster, although the observed Cu–Cu distances are typical of those seen for Cu–thiolate clusters [70].

For the Cu chaperone hCCS, which is responsible for insertion of Cu into superoxide dismutase, EXAFS data for a di-copper form of the protein showed an average Cu environment of three sulfur scatterers at 2.26 Å and a Cu–Cu distance of 2.72 [72]. These data demonstrated that the Cu forms a dinuclear site, and suggested that there are two doubly bridging cysteine ligands. When combined with sequence data, these results suggested that a Cu cluster forms a bridge between domains I and III of the protein [72].

Despite numerous successes, caution is necessary in interpreting EXAFS evidence for cluster structures. The absence of outer shell scattering does not necessarily indicate the absence of outer shell metals. Thus, while Cu metallothionein has intense outer-shell scattering [65], the zinc, cadmium, and mercury bound forms of metallothionein lack significant outer-shell peaks [73], despite the presence of multinuclear clusters for all four metals. In part, this may reflect differences in the temperatures used for the measurements (4–8 K for Cu versus 77 K for the other samples). It may also reflect differences in ligation: mixed digonal and trigonal for Cu versus tetrahedral for Zn and Cd, although Hg also appears to have a distorted digonal ligation but to lack detectable Hg–Hg scattering. Perhaps the most important factor affecting the detectability of metal–metal scattering is the extent of disorder in the cluster; if there are a range of different metal–metal distances rather than the single metal–metal distance that is often seen in highly symmetric model compounds, this will significantly reduce the amplitude of the metal–metal scattering.

It is certainly the case that Zn–Zn EXAFS signals *can* be observed. In neuronal-growth-inhibitory factor (GIF), a metalloprotein with 70% sequence identity to metallothionein, there is a clear Zn–Zn EXAFS signal at ca. 3.28 Å [74]. However, although both metallothionein and GIF both bind seven metals atoms, GIF is isolated with both Cu and Zn in a ratio of 4:3 while the metallothionein samples discussed above all contained only a single metal ion. Thus, if disorder is important for determining the detectability of Zn–Zn scattering, it is likely to be more severe for metallothionein than for GIF.

In GIF, the Zn–Zn distance is very similar to that seen for $(Cys)_2Zn(\mu\text{-}Cys)_2Zn(Cys)_2$ dimers, suggesting that GIF may contain this structural unit. The GIF data were measured at 77 K demonstrating that such structural features can be detected at this temperature and thus suggesting that the Zn cluster in metallothionein does not contain this unit. Interestingly, the Cu EXAFS data for GIF showed metal–metal EXAFS at ca. 2.7 Å while no 2.7 Å feature was seen in the Zn EXAFS for GIF. Although the 2.7 Å feature in the Cu EXAFS could, in principle, be due to either Cu–Cu or Cu–Zn scattering, the absence of a corresponding feature in the Zn EXAFS suggests that the Cu and Zn must be segregated into distinct clusters. This illustrates once again the value of making EXAFS measurements at multiple absorption edges.

In addition to the possibility that a multinuclear cluster may fail to show a detectable metal–metal EXAFS signal, there are also potential difficulties in assigning the identity of the outer-shell signals that are seen. For example, the binuclear mixed valence Cu–A site is now known to have a Cu–Cu separation of 2.4 Å [75]. However, the initial EXAFS studies of Cu–A sites did not report a detectable Cu–Cu signal [76–79]. Rather, they reported an unusually long Cu–(S/Cl) feature at ca. 2.6 Å [76–78] which, with the benefit of hindsight, now appears to have been misidentified Cu–Cu scattering. Similarly, the EXAFS data for the di-zinc site in the regulatory protein Gal4 was originally interpreted as indicating that the Zn was coordinated to three sulfurs at 2.30 Å and one oxygen at 1.95 Å, with an unusually long

Zn–S interaction at 3.34 Å [80]. The latter is actually due to Zn–Zn scattering at ca. 3.16 Å, such as that seen in the related protein Prp1 [81], while the nearest-neighbor scattering is now known to arise exclusively from sulfur. For both Cu–A and Gal4, a previously unanticipated metal–metal interaction was initially mis-identified as metal-S/Cl scattering, thus highlighting the difficulty of making unambiguous assignments of outer-shell EXAFS. This can severely limit the utility of EXAFS for determining metal-cluster nuclearity [29].

4. XANES studies of proteins

In the XANES region, multiple-scattering effects are much more pronounced. The X-ray excited photoelectron has a much lower energy than in the EXAFS region. This results in a much longer mean-free-path for the photoelectron, allowing the photoelectron to sample a much larger volume around the absorber. This is both a blessing, since it means that XANES has greater sensitivity to geometry, and a curse, since it makes quantitative interpretation of XANES spectra much more challenging. Much of the recent interest in XANES spectroscopy stems from the hope that careful analysis of XANES spectra can be used to determine three-dimensional structure of the absorbing site. Although there has been recent progress in theoretical simulations of XANES spectra [82–85], it remains the case that most XANES simulations do not do a very good job of reproducing the subtle features of the spectrum. For this reasons, most XANES analyses rely on qualitative rather than quantitative interpretation.

In comparing XANES spectra between publications, it is important to note that different methods may be used both to normalize the spectra and to determine the energy calibration. Spectra can be normalized by setting the edge jump (i.e., the difference between the absorbance below the edge and above the edge) to be 1, or by matching to absolute X-ray absorption cross-sections. Examples of both are shown in Figs. 8 and 9. In most studies, absolute X-ray energies are not known. Rather, the X-ray energy is calibrated by reference to some internal standard, often a foil of the relevant metal. Although this does not give absolute X-ray energies, and may not permit comparison between different studies, it does permit comparison of spectra within a single study. Finally, depending on the experimental details, there may be differences in spectral resolution that complicate direct comparison of spectra measured by different groups and at different times.

4.1. Determination of ligation

XANES spectra change depending on the identity of the ligand and this can be used to provide at least qualitative information about the ligation of an unknown site. An example of the dependence of XANES spectra on ligation is shown in Fig. 8 [86]. For citrate, which is expected to give a relatively symmetric site with oxygen ligation, there is an intense “white line” at ca. 9670 eV. For histidine, which is expected to give a zinc that is coordinated by four nitrogens, possibly with additional ligation by two carboxylate oxygens, the white line is weaker, but occurs at approximately the same energy. In contrast, sulfur ligation gives a much less intense white line that is shifted to lower energy. The difference between citrate and histidine can be explained as a consequence of disorder; as the ligation environment becomes less symmetric, the scattering resonances that give rise to the XANES features are broadened, giving a less intense white-line [87]. The lower intensity for the sulfur white-lines may reflect fact that the Zn is tetrahedral in these cases, thus giving four rather than six scattering atoms to contribute to the white-line intensity. The shift to lower en-

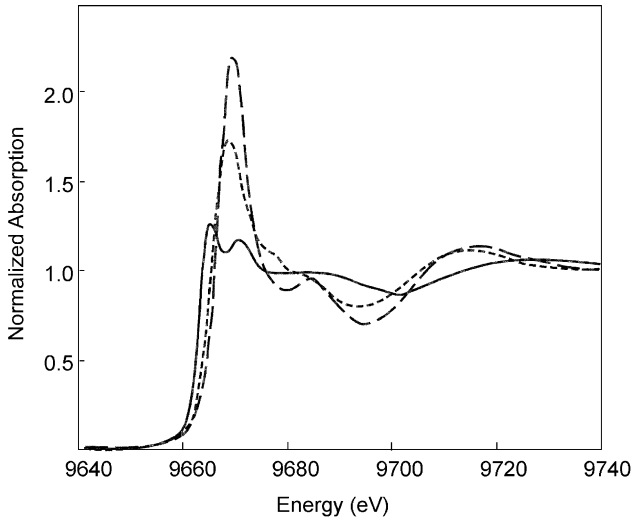

Fig. 8. XANES spectra for aqueous solutions of Zn citrate (dashed line), Zn histidine (dotted line), and Zn cysteine (solid line). Redrawn from data in [86].

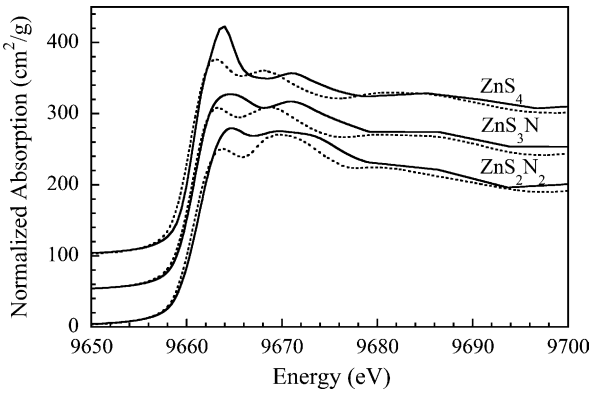

Fig. 9. XANES spectra for tetrahedral Zn models showing the effect of S vs. N ligation. Solid lines are for crystallographically characterized models; dotted lines are for Zn bound to the Zn-finger consensus peptide. Redrawn from data in [34].

ergy when there are sulfur ligands has been interpreted in terms of charge transfer from ligand to metal [86]. While this may account for some of the shift (see Section 4.3), most of the shift is probably a consequence of the fact that Zn–S bonds are longer than Zn–(O/N) bonds. Theoretically, the edge energy is expected vary inversely with the square of the metal–ligand distance [88].

Although the trends in Fig. 8 can be used as a "fingerprint" for identifying an unknown, care has to be used in drawing structural conclusions from XANES spectra. The difficulty is illustrated by Fig. 9, which compares the XANES spectra for several different tetrahedral Zn complexes (note that the data in Fig. 9 are normalized to absolute absorption cross-sections, while that in Fig. 8 is normalized to a unit edge jump) [34]. It is clear, at least for the edges in Fig. 9, that the presence of nitrogen ligands has almost no effect on the edge energy for mixed S–N ligation.

The white-line feature at approximately 9664 eV, which is most intense for the ZnS_4 sites, has been used as a marker for Zn–tetrathiolate ligation. However, the intensity of this feature is quite variable, even for compounds with identical ligation (i.e., identical EXAFS spectra). In general, all of the XANES features are more pronounced for the crystalline small-molecule models than for their peptide analogs. This may reflect the higher symmetry of the small-molecule models, consistent with the variations in Fig. 8. Regardless of the origin of this variation, it greatly complicates the use of XANES as a fingerprint since, at least for the tetrahedral complexes in Fig. 9, the variation in edge structure from sample to sample within a single ligation type is larger than the variation due to ligation [34]. This sensitivity to minor structural variations illustrates both the attractions, but also the challenges of trying to use XANES to determine geometrical structure.

4.2. Determination of coordination number

As suggested by Fig. 8, there are changes in the Zn XANES as the coordination number changes. This is a general property of XANES, but is especially dramatic for Cu. The Cu XANES spectrum has an intense transition before the main edge, as shown in Fig. 10. This pre-edge transition has been attributed to a 1s → 4p transition [89]. For Cu(I), the pre-edge transition occurs at ca. 8984 eV, while for Cu(II), it shifts to approximately 8987 eV, where it is often obscured by the rising edge. This has been used as an indicator of the presence of Cu(I) [90], for example, to distinguish between an antiferromagnetically coupled Cu(II) dimer and a Cu(I) site, both of which are EPR silent. Within Cu(I) sites, there is tremendous variation in the intensity of the pre-edge transition. This is illustrated in Fig. 10, with the comparison of the XANES for PcoC, a protein that contains a three-coordinate CuS_2(N/O) site [91] and CueR, a protein with a digonal CuS_2 site [69]. This sensitivity of Cu XANES to geometry has proven particularly useful in recent studies of metallochaperones [69,72,91–96], where conversion from a two-coordinate site to a three-coordinate site may play an important mechanistic role in Cu transport and delivery [96].

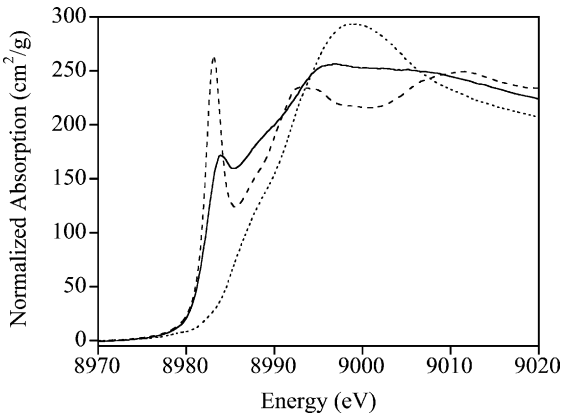

Fig. 10. Comparison of Cu XANES spectra for Cu(I) PcoC (solid line, three-coordinate CuS_2(N/O) site [91]) and Cu(I) CueR (dashed line, two-coordinate Cu site [69]). For reference, the XANES spectrum for the Cu(II) form of PcoC is also shown (dotted line).

4.3. Determination of oxidation state

As illustrated by Fig. 10, the energy of the X-ray absorption edge depends on the oxidation state of the absorbing atom. This can often be used to determine metal-ion oxidation state, although care must be used since, as shown in Fig. 8, ligation can also affect edge energy. Determination of metal-ion oxidation state is seldom of direct interest for spectroscopically quiet metals—many metals (e.g., Zn, Cd, Hg,) have only one biologically accessible oxidation state. Others, such as Cu, can exist in multiple oxidation states, but the distinction between these is straightforward using conventional spectroscopies. However, XANES spectra appear to also be sensitive to more subtle changes in electronic structure. For the Zn-containing alkyl-transfer enzymes [97], including methionine synthase (Section 3.1), there is a small but reproducible shift in the Zn edge energy when the thiolate substrate binds to the Zn [59]. This can be seen most easily by calculating the difference spectrum. The difference of enzyme minus enzyme + substrate (Fig. 11) shows a characteristic bimodal feature at the edge (ca. 9660 eV), due to the fact that there is a very small shift of the edge to lower energy when substrate binds [59]. This shift is comparable to the shifts seen for different ligation types (e.g., Figs. 8 and 9), and thus could conceivably be due to the fact that substrate binding results in displacement of a low-Z (O/N) ligand with a sulfur ligand. However, identical spectral changes are seen when either Hcy or Se-Hcy bind (see Fig. 11). This rules out the possibility that the differences are due to changes in ligation, since in one case a sulfur ligand is added while in the other a selenium ligand is added. Although the Zn oxidation state does not change, it is possible that there is a slight decrease in the local charge on the

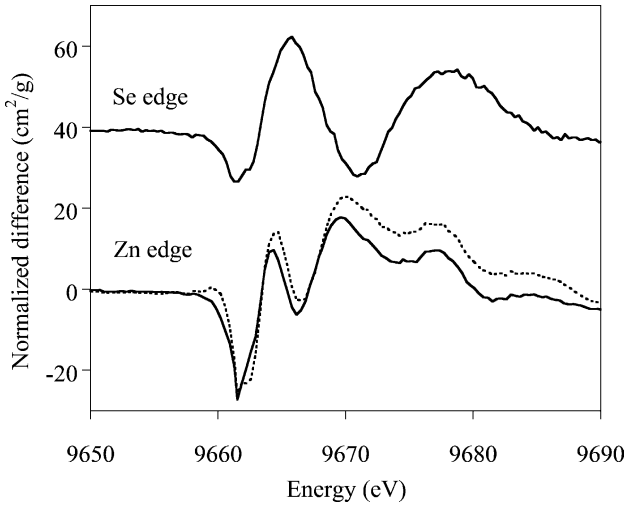

Fig. 11. XANES difference spectra for MetE methionine synthase. Lower spectra are the difference spectra for the native protein minus the spectrum for the protein + substrate. Solid line: Hcy substrate; dashed line: Se–Hcy substrate. Top spectra are the corresponding difference for the Se edge (calculated as SeHcy + MetE − SeHcy). Se spectra are shifted vertically by 40 and horizontally by −2997 eV for clarity. Redrawn from data in [59].

Zn when substrate binds, and that this causes the slight decrease in the Zn edge energy. Support for this interpretation comes from the Se edge, which shows a corresponding shift to slightly higher energy when Se-Hcy is bound to MetE [59]. For comparison of the difference spectra (Fig. 11), the Se difference was calculated as SeHcy + MetE minus Se-Hcy, so that the shift of the Se edge to higher energy again appears as a negative feature in the difference spectrum. The intrinsic line-width of absorption edge increases as energy increases, thus Se K-edges (12.6 keV) are somewhat broader than Zn K-edges (9.6 keV), making the difference features somewhat broader for Se. Although this broadening is apparent in Fig. 11, the overall appearance at the edge is very similar for Zn and Se. The difference features at higher energy depend on multiple scattering and are thus quite different when viewed from the Zn edge or the Se edge.

5. XAS studies of crystalline proteins

One of the key attractions of XAS is its ability to provide structural information about non-crystalline systems. Even in the era of structural genomics, this continues to be important since many proteins fail to give diffraction quality crystals. In yet other cases, diffraction quality crystals exist, but have metal-sites that are disordered [98,99]. In other cases, crystals may be available, but the structural questions of interest involve *solution* structure (for example, the structure of a reactive intermediate, as discussed in Section 6).

However, there are also cases in which XAS can play a critical role, even though a crystal structure is available for the metal site. One obvious application is in determination of oxidation state. Since XANES spectra are typically quite sensitive to oxidation state, they can be used to determine the oxidation state of the metal in the crystal that was used for X-ray diffraction. This is unique information that is generally impossible to obtain crystallographically.

A second application involves the use of EXAFS to determine bond lengths. For a crystal that diffracts to 2 Å, the uncertainty in metal–ligand distance is expected to be 0.3 Å or more [100]. This is much larger than the uncertainty associated with EXAFS bond lengths, and can be so large that it is impossible to understand critical features of the metal site based on crystallography alone. An example of this for the protein farnesyl transferase is given below.

Farnesyltransferase (FTase) catalyzes the transfer of the farnesyl group of farnesyl diphosphate to the cysteine in a C-terminal CaaX sequence of the target protein [101–103]. A total of 10 crystal structures have been reported for FTase, all at a resolution of 2.0 Å or worse. There is a single Zn in the FTase active site, bound to Asp 297, His 362, Cys 299, and a water molecule when the enzyme is in its resting state [102]. The crystallographically determined zinc-ligand distances for the two different FTase + FPP structures, the five different FTase ternary complexes, and the two different FTase product complexes all differ significantly, reflecting the relatively poor precision of 2 Å crystal structures.

Many of the crystallographic Zn–ligand distances are substantially longer than the Zn–ligand distances that are found in small molecules. For example, the typical Zn–O (water and carboxylate) and Zn–N (histidine) distances for a four-coordinate Zn are 2.00–2.04 Å, while typical Zn–S distances are 2.29 Å [104]. In comparison, the average Zn–(N/O) distance for the FTase crystal structures varies (depending on the structure) from 2.22 to 2.45 Å while the Zn–S distance varies from 2.22 to 2.52 Å [37]. The latter is potentially important, since it is possible that the protein strains (and thus lengthens) the Zn–S distance in the ternary complex. This could play an important role in activating the peptide cysteine thiolate for nucleophilic attack on the farnesyl diphosphate. EXAFS measurements were used to determine the Zn–ligand distances with greater accuracy than was possible crystallographically. In all cases, the EXAFS derived bond lengths were shorter than the crystallographic bond lengths, but were completely consistent with those expected from the equivalent small molecule crystal structures.

The EXAFS data also helped to resolve the question of whether the Zn site is four- or five-coordinate in FTase, since both had been found crystallographically. The EXAFS data showed that both the Zn–S distance and the Zn–(N/O) distance were nearly identical in all forms of the protein [37]. This suggested that there is no change in the coordination number of the zinc during catalysis and, based on the observed bond length, that the Zn is four-coordinate in each form of the enzyme.

In the FTase example, XAS data were analyzed independently of analyses of X-ray diffraction data. It is also possible to combine both crystallographic and EXAFS data into a single analysis. This approach was used in a study of azurin [105], a blue copper protein in which the Cu is coordinated to two histidines, one cysteine, one methionine, and a backbone carbonyl from a glycine. Since the EXAFS data were only analyzed over 3.5–11.5 $Å^{-1}$ ($N_{idp} \approx 15$), it was not realistic to refine parameters for all five ligands (>20 adjustable parameters) without some additional source of restraints. Even though diffraction data was available to relatively high resolution (1.75 Å), the crystallographic coordinates did not reproduce the EXAFS data. A rigid body refinement, with the intra-ligand structure held fixed, significantly improved the fit with only small (ca. 0.05 Å) variations in metal–ligand distances, and a full three-dimensional refinement, using the crystallographic data to provide additional restraints [106], gave a further improvement in the fit. While it is not clear that all of the refined parameters are meaningful (for example, the Cu–S(Met) interaction has a Debye–Waller factor of 0.029 $Å^2$, meaning that its EXAFS contribution is damped by a factor of 50 by $k = 8\,Å^{-1}$), this approach remains a promising method to combine the strengths of crystallography (three-dimensional structure) with those of EXAFS (accurate bond lengths).

6. Time-resolved XAS

In addition to static measurements, it is relatively straightforward to use XAS in combination with rapid mixing apparatus to study reacting systems in real-time. By providing real-time structural information, time-resolved XAS can be extraordinarily useful for mechanistic studies. However, although there are hundreds of papers on time-resolved XAS, most deal with samples from materials science and catalysis, rather than from biological systems, due to the difficulty of obtaining good time-resolved XAS on dilute samples.

The best time resolution comes from a "dispersive" geometry [107], in which a polychromatic X-ray beam is focused onto the sample of interest. Unfortunately, the dispersive geometry is limited to relatively high metal concentrations (>10 mM for modest time resolution; higher for ms time resolution) and is thus not practical for most biological samples [108]. XAS studies of dilute samples generally require that the data be measured as fluorescence excitation spectra and are thus incompatible with dispersive measurements. Fluorescence measurements require that the excitation wavelength be scanned, and even with recent advances in rapid scanning monochromators, it has not proven possible to measure XAS spectra with scan times better than ca. 50 ms [109] and typical scan times are several seconds [110]. Despite these limitations, time-resolved XAS is beginning to have an impact on biological studies, particularly with the high flux capabilities of third-generation synchrotrons.

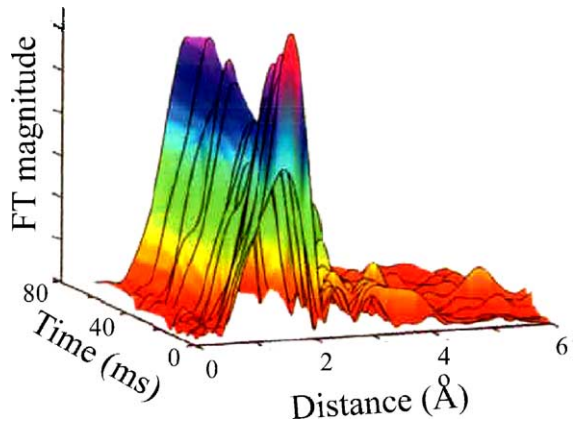

Fig. 12. Fourier transforms of time-resolved EXAFS data for RFQ-trapped samples of alcohol dehydrogenase, showing the change in structure during the first 80 ms of the reaction. Redrawn from data in [112].

There are two main applications of time-resolved studies: structural characterization of intermediates and determination of kinetic constants.

6.1. Structure of intermediate states

A reactive intermediate is difficult or impossible to crystallize, since crystallization inevitably requires significant time. Although in rare cases it is possible to generate intermediates in situ in a crystal, it remains the case that most intermediates require spectroscopic rather than crystallographic characterization. Depending on reaction rates, preparation of an intermediate state may be as straightforward as adding the substrate and freezing the sample for study by conventional XAS. More often, it is necessary to prepare samples using rapid-freeze-quench (RFQ) to trap samples at various stages along the reaction pathway [111]. This was used recently to follow the complete time-course of the reaction of alcohol dehydrogenase [112] by trapping 20 different samples with reaction times varying from ca. 2 ms (the mixing time of the apparatus) to 110 ms (see Fig. 12). Since the system evolves continuously during the reaction, with many different species present, none of the resulting spectra represent a literal "snapshot" of an intermediate. However, by combining multiple spectra, it is possible to extract mathematically the principal components responsible for the spectral variation, even for components that are only ever present as a minority of the absorbing species [113–118]. This approach allowed the authors to extract spectra that were proposed to represent two different five-coordinate intermediates that form sequentially during the first 70 ms of the reaction. These data suggested that there is a previously unanticipated structural change in the Zn site during the early phase of the reaction. Although the data are relatively noisy, and additional work will be required to confirm the structural conclusions, this study clearly demonstrates the potential of time-dependent studies for structural characterization of intermediates.

6.2. Determination of kinetic constants

In the example above, time-resolved XAS is not significantly different from conventional XAS—it is only the sample preparation that is different. A very different approach to time-resolved XAS is to determine reaction kinetics. While this is not necessarily important for many proteins, where it may be substantially easier to measure reaction kinetics using conventional spectroscopies (e.g., stopped-flow UV-Vis spectroscopy), time-resolved XAS may be the only way to measure the rate constants for spectroscopically quiet metals. An early example of this was the use of XAS to determine the reaction rate for decomposition of the intermediate that is formed when carboxypeptidase is mixed with the slow substrate Z-Sar-Phe [119]. In this case, the reaction was slow enough (hours) that conventional fluorescence XAS measurements could be completed on a time scale (3–5 min) that was short compared to the reaction rate. The XAS data were fit to a first-order kinetic model, giving reaction rates of $6 \times 10^{-4}\ s^{-1}$ at 15 °C and $2 \times 10^{-4}\ s^{-1}$ at 5 °C. Prior work had determined the reaction rate for this substrate with the Co-substituted enzyme, but was unable to probe directly the reaction rate for the native Zn enzyme [120]. Interestingly, the reaction was much slower with the native Zn than it was with Co.

In order to have better time resolution, it is generally necessary to restrict the measurements to a single wavelength [121], rather than measuring the complete X-ray absorption spectrum. Recently, this has been used with for ms time-resolved studies of alcohol dehydrogenase [112]. Data measured at a single X-ray wavelength (selected from model studies and from the static RFQ data discussed above), confirmed the existence of two distinct phases during the first 100 ms of the reaction of alcohol dehydrogenase with propanol. Conventional stopped flow measurements under comparable conditions but using UV-Vis absorbance to monitor $NADP^+$ reduction, showed only a single phase in this time regime. While there have been a few other uses of this approach, for example measurements of the rate of photoreduction ($0.57\ min^{-1}$) of the Mn cluster in the photosynthetic oxygen evolving complex [110], this approach has not yet found wide application to biological samples. However, as the capabilities of synchrotron sources continue to develop, one can anticipate a significant increase in XAS-based kinetic measurements.

7. In situ studies

Most of the examples discussed thus far have involved homogeneous samples. However, since XAS can be used to study any form of matter, there is no need to limit studies to purified samples. Thus, for example, EXAFS measurements of rabbit plasma were able to show that co-administration of mercuric chloride and sodium selenite results in formation of a Hg–S–Se cluster in the plasma [122]. Other spectroscopic probes such as Raman spectroscopy, ^{199}Hg NMR and ^{77}Se NMR had all been inconclusive, and no peaks attributable to Hg or Se were observed in the mass spectrum of the serum, perhaps due to the lability of the cluster. The evidence for a Hg–S–Se cluster provides insight into the unusual antagonism between inorganic mercury and selenium, both of which are toxic, but which have greatly reduced toxicity when administered together.

In the Hg/selenite system, it appeared that virtually all of the Hg and Se were present in the cluster based on comparison with model systems, and thus this system may have been effectively homogeneous, even though the cluster was not purified from the serum. However, in situ XAS can also be used to samples that are significantly heterogeneous. For example, several studies have used in situ XAS characterize the oxidation state and average environment of metal ions in a variety of plants that act as metal hyper-accumulators [86,123,124]. These studies are of necessity limited by the fact that XAS is an averaging method, and thus gives only the average metal environment. Nevertheless, these have been useful to begin investigating the mechanism of metal uptake and storage.

A third example of in situ XAS spectroscopy is a study of the chemical speciation of Zn, which is found at ca. 1 mM concentration in *Xenopus* oocytes [125]. In early stage embryos, the average Zn environment resembles the $ZnHis_2Cys_2$ site in zinc-finger proteins, while as the oocytes develop, the predominant zinc species becomes one that has primarily low-*Z* ligation, as found, for example, in the $ZnHis_2(N/O)_2$ site in the Zn carrier protein lipovitellin.

These studies demonstrate the tremendous potential of XAS for in situ studies of intact biological systems, in which the metal is present in a complex, multicomponent mixture. The ability to extract detailed structural data depends on the complexity of the system. In cases where samples can be systematically varied, for example by examining different developmental stages in the case of oocyte maturation, it should be possible to extract information about metal speciation using the same kind of multiple-component analysis that was used for time-dependent studies. In other cases, in situ XAS may be limited to providing information about the average structure, although even here the XAS data may provide unique insight that is not available from other methods.

A particularly exciting new opportunity is to combine in situ, or perhaps even in vivo XAS measurements with an X-ray microprobe. It is now possible, using third generation synchrotrons, to produce extremely intense X-ray beams with a sub-micron beam size. Small beams allow spatially-resolved XAS data to be measured on intact biological samples [126,127]. This can significantly simplify interpretation of the XAS, allowing, for example, determination of the distribution of different oxidation states across an organism. Recent results have even been able to extend XAS to the single-cell level [128,129]. When combined with tomographic reconstructions, this should allow determination

of the three-dimensional distribution of different chemical forms of an element within a sample [130].

8. Prospects for the future

The number of proteins that have been isolated continues to increase, largely as a consequence of worldwide structural genomics efforts. Many of these proteins will be found to bind spectroscopically quiet metals, and this alone guarantees that XAS will continue to play an important role in bioinorganic chemistry. In addition, recent progress with both time-resolved and in situ measurements suggests that important new areas of application of XAS are likely to open in the future. With the development of third-generation synchrotron sources, it has become possible to measure X-ray absorption spectra for smaller volumes and to measure the spectra more quickly. This, coupled to the small size X-ray beams that can be produced using third-generation sources, is likely to open new opportunities for detailed spatially-resolved and temporally-resolved spectroscopy.

Acknowledgements

This research was supported in part by NIH Research Grant GM38047. My work with synchrotron radiation has made use of SSRL, NSLS, and APS, all of which are supported by the Department of Energy, Office of Basic Energy Sciences, with additional support from the National Institutes of Health, National Center for Research Resources, Biomedical Technology Program, and by the Department of Energy, Office of Biological and Environmental Research.

References

[1] S.E. Shadle, B. Hedman, K.O. Hodgson, E.I. Solomon, Inorg. Chem. 33 (1994) 4235.
[2] S.E. Shadle, B. Hedman, K.O. Hodgson, E.I. Solomon, J. Am. Chem. Soc. 117 (1995) 2259.
[3] F. Neese, B. Hedman, K.O. Hodgson, E.I. Solomon, Inorg. Chem. 38 (1999) 4854.
[4] T. Glaser, B. Hedman, K.O. Hodgson, E.I. Solomon, Acc. Chem. Res. 33 (2000) 859.
[5] B. Hedman, E.I. Solomon, Coord. Chem. Rev., in this issue.
[6] L.M. Utschig, J.G. Wright, T.V. O'Halloran, Methods Enzymol. 226 (1993) 71.
[7] R.A. Santos, E.S. Gruff, S.A. Koch, G.S. Harbison, J. Am. Chem. Soc. 113 (1991) 469.
[8] G.A. Bowmaker, R.K. Harris, S.W. Oh, Coord. Chem. Rev. 167 (1997) 49.
[9] H.G. Fijolek, T.A. Oriskovich, A.J. Benesi, P. GonzalezDuarte, M.J. Natan, Inorg. Chem. 35 (1996) 797.
[10] W. Troger, T. Butz, Hyperfine Interac. 129 (2000) 511.
[11] A.S. Lipton, C. Bergquist, G. Parkin, P.D. Ellis, J. Am. Chem. Soc. 125 (2003) 3768.
[12] A.S. Lipton, T.A. Wright, M.K. Bowman, D.L. Reger, P.D. Ellis, J. Am. Chem. Soc. 124 (2002) 5850.
[13] F.H. Larsen, A.S. Lipton, H.J. Jakobsen, N.C. Nielsen, P.D. Ellis, J. Am. Chem. Soc. 121 (1999) 3783.
[14] I. Bertini, C. Luchinat, Met. Ions Biol. Syst. 15 (1983) 101.
[15] I. Bertini, C. Luchinat, Bioinorganic Chemistry, University Science Books, Mill Valley, CA, 1994, p. 37.
[16] M.F. Summers, Coord. Chem. Rev (1988).
[17] J.E. Coleman, Annu. Rev. Biochem. 61 (1992) 897.
[18] S.S. Narula, D.R. Winge, I.M. Armitage, Biochemistry 32 (1993) 6773.
[19] P.A. Cobine, G.N. George, D.J. Winzor, M.D. Harrison, S. Mogahaddas, C.T. Dameron, Biochemistry 39 (2000) 6857.
[20] C. Kimblin, B.M. Bridgewater, D.G. Churchill, T. Hascall, G. Parkin, Inorg. Chem. 39 (2000) 4240.
[21] A. Kremer-Aach, W. Kläui, R. Bell, A. Strerath, H. Wunderlich, D. Mootz, Inorg. Chem. 36 (1997).
[22] S.P. Cramer, Chem. Anal. 92 (1988) 257.
[23] E.D. Crozier, Nucl. Instrum. Methods Phys. Res. B 133 (1997) 134.
[24] C.D. Garner, Applications of Synchrotron Radiation, Blackie, Glasgow, 1990, p. 268.
[25] D.C. Koningsberger, R. Prins (Eds.), X-ray Absorption: Principles, Applications, Techniques of EXAFS, SEXAFS, and XANES, Wiley, New York, 1988.
[26] P.A. Lee, P.H. Citrin, P. Eisenberger, B.M. Kincaid, Rev. Mod. Phys. 53 (1981) 769.
[27] R.A. Scott, Methods Enzymol. 117 (1985) 414.
[28] B.K. Teo, EXAFS: Basic Principles and Data Analysis, Springer-Verlag, New York, 1986.
[29] P.J. Riggs-Gelasco, T.L. Stemmler, J.E. Penner-Hahn, Coord. Chem. Rev. 144 (1995) 245.
[30] J.E. Penner-Hahn, Coord. Chem. Rev. 192 (1999) 1101.
[31] M. Vaarkamp, I. Dring, R.J. Oldman, E.A. Stern, D.C. Koningsberger, Phys. Rev. B 50 (1994) 7872.
[32] J.J. Rehr, d.L.J. Mustre, S.I. Zabinsky, R.C. Albers, J. Am. Chem. Soc. 113 (1991) 5135.
[33] J.J. Rehr, R.C. Albers, S.I. Zabinsky, Phys. Rev. Lett. 69 (1992) 3397.
[34] K. Clark-Baldwin, D.L. Tierney, N. Govindaswamy, E.S. Gruff, C. Kim, J. Berg, S.A. Koch, J.E. Penner-Hahn, J. Am. Chem. Soc. 120 (1998) 8403.
[35] P.J. Riggs-Gelasco, R. Mei, C.F. Yocum, J.E. Penner-Hahn, J. Am. Chem. Soc. 118 (1996) 2387.
[36] C.P. McClure, K.M. Rusche, K. Peariso, J.E. Jackman, C.A. Fierke, J.E. Penner-Hahn, J. Inorg. Biochem. 94 (2003) 78.
[37] D.A. Tobin, J.S. Pickett, H.L. Hartman, C.A. Fierke, J.E. Penner-Hahn, J. Am. Chem. Soc. 125 (2003) 9962.
[38] M. Kruer, M. Haumann, W. Meyer-Klaucke, R.K. Thauer, H. Dau, Eur. J. Biochem. 269 (2002) 2117.
[39] G. Bunker, S. Hasnain, D. Sayers, X-ray Absorption Fine Structure, Ellis Horwood, New York, 1991, p. 751.
[40] E.A. Stern, Phys. Rev. B 48 (1993) 9825.
[41] A. Michalowicz, G. Vlaic, J. Synchrot. Radiat. 5 (1998) 1317.
[42] S. Wang, M.H. Lee, R.P. Hausinger, P.A. Clark, D.E. Wilcox, R.A. Scott, Inorg. Chem. 33 (1994) 1589.
[43] R.W. Strange, N.J. Blackburn, P.F. Knowles, S.S. Hasnain, J. Am. Chem. Soc. 109 (1987) 7157.
[44] M.J. Latimer, V.J. DeRose, I. Mukerji, V.K. Yachandra, K. Sauer, M.P. Klein, Biochemistry 34 (1995) 10898.
[45] F.W. Lytle, D.E. Sayers, E.A. Stern, Physica B 158 (1988) 701.
[46] R.W. Joyner, K.J. Martin, P. Meehan, J. Phys. C: Solid State Phys. 20 (1987) 4005.
[47] N.J. Blackburn, S.S. Hasnain, T.M. Pettingill, R.W. Strange, J. Biol. Chem. 266 (1991) 23120.
[48] P.W. Loeffen, R.F. Pettifer, Phys. Rev. Lett. 76 (1996) 636.
[49] P.W. Loeffen, R.F. Pettifer, Physica B 209 (1995) 39.
[50] P. Lay, A. Levina, R. Armstrong, Coord. Chem. Rev. 249 (2005) 14.

[51] K. Clark-Baldwin, A.R. Johnson, Y.W. Chen, E.E. Dekker, J.E. Penner-Hahn, Inorg. Chim. Acta 276 (1998) 215.
[52] G.W. Buchko, N.J. Hess, V. Bandaru, S.S. Wallace, M.A. Kennedy, Biochemistry 39 (2000) 12441.
[53] K. Clark, Ph.D. thesis, The University of Michigan, 1993.
[54] J.C. Gonzalez, C.W. Goulding, J.T. Jarrett, K. Peariso, J.E. Penner-Hahn, R.G. Matthews, Protein Eng. 10 (1997) 57.
[55] J.C. González, R.V. Banerjee, S. Huang, J.S. Sumner, R.G. Matthews, Biochemistry 31 (1992) 6045.
[56] J.C. Gonzalez, K. Peariso, J.E. Penner-Hahn, R.G. Matthews, Biochemistry 35 (1996) 12228.
[57] Z.H.S. Zhou, K. Peariso, J.E. Penner-Hahn, R.G. Matthews, Biochemistry 38 (1999) 15915.
[58] G.A. Garcia, D.L. Tierney, S.R. Chong, K. Clark, J.E. PennerHahn, Biochemistry 35 (1996) 3133.
[59] K. Peariso, Z.H.S. Zhou, A.E. Smith, R.G. Matthews, J.E. Penner-Hahn, Biochemistry 40 (2001) 987.
[60] I.D. Brown, J. Chem. Educ. 53 (1976) 100.
[61] I.D. Brown, J. Chem. Educ. 53 (1976) 231.
[62] I.D. Brown, D. Altermatt, Acta Crystallogr. Sect. B: Struct. Commun. 41 (1985) 244.
[63] W.T. Liu, H.H. Thorp, Inorg. Chem. 32 (1993) 4102.
[64] H.H. Thorp, Inorg. Chem. 31 (1992) 1585.
[65] I.J. Pickering, G.N. George, C.T. Dameron, B. Kurz, D.R. Winge, I.G. Dance, J. Am. Chem. Soc. 115 (1993) 9498.
[66] A. Presta, A.R. Green, A. Zelazowski, M.J. Stillman, Eur. J. Biochem. 227 (1995) 226.
[67] M.J. Stillman, Coord. Chem. Rev. 144 (1995) 461.
[68] N.J. Blackburn, M. Ralle, E. Gomez, M.G. Hill, A. Pastuszyn, D. Sanders, J.A. Fee, Biochemistry 38 (1999) 7075.
[69] K. Chen, S. Yuldasheva, J.E. Penner-Hahn, T.V. O'Halloran, J. Am. Chem. Soc. 125 (2003) 12088.
[70] D.N. Heaton, G.N. George, G. Garrison, D.R. Winge, Biochemistry 40 (2001) 743.
[71] K.R. Brown, G.L. Keller, I.J. Pickering, H.H. Harris, G.N. George, D.R. Winge, Biochemistry 41 (2002) 6469.
[72] J.F. Eisses, J.P. Stasser, M. Ralle, J.H. Kaplan, N.J. Blackburn, Biochemistry 39 (2000) 7337.
[73] D.T. Jiang, S.M. Heald, T.K. Sham, M.J. Stillman, J. Am. Chem. Soc. 116 (1994) 11004.
[74] R. Bogumil, P. Faller, P.A. Binz, M. Vasak, J.M. Charnock, C.D. Garner, Eur. J. Biochem. 255 (1998) 172.
[75] N.J. Blackburn, M.E. Barr, W.H. Woodruff, J. Vanderooost, S. Devries, Biochemistry 33 (1994) 10401.
[76] D.M. Dooley, M.A. McGuirl, A.C. Rosenzweig, J.A. Landin, R.A. Scott, W.G. Zumft, F. Devlin, P.J. Stephens, Inorg. Chem. 30 (1991) 3006.
[77] G.N. George, S.P. Cramer, T.G. Frey, R.C. Prince, Biochim. Biophys. Acta 1142 (1993) 240.
[78] R.A. Scott, W.G. Zumft, C.L. Coyle, D.M. Dooley, Proc. Natl. Acad. Sci U.S.A. 86 (1989) 4082.
[79] C.K. SooHoo, C.K. Hollocher, A.F. Kolodziej, W.H. Orme-Johnson, G. Bunker, J. Biol. Chem. 266 (1991) 2210.
[80] J.F. Povey, G.P. Diakun, C.D. Garner, S.P. Wilson, E.D. Laue, FEBS Lett. 266 (1990) 142.
[81] L.J. Ball, G.P. Diakun, P.L. Gadhavi, N.A. Young, E.M. Armstrong, C.D. Garner, E.D. Laue, FEBS Lett. 358 (1995) 278.
[82] M. Benfatto, A. Congiu-Castellano, A. Daniele, S.D. Longa, J. Synchrot. Radiat. 8 (2001) 267.
[83] M. Benfatto, S. Della Longa, J. Synchrot. Radiat. 8 (2001) 1087.
[84] M. Benfatto, S. Della Longa, C.R. Natoli, J. Synchrot. Radiat. 10 (2003) 51.
[85] M. Benfatto, P. D'Angelo, S. Della Longa, N.V. Pavel, Phys. Rev. B 65 (2002).
[86] R.A. Kelly, J.C. Andrews, J.G. DeWitt, Microchem. J. 71 (2002) 231.
[87] T.L. Stemmler, T.M. Sossong, J.I. Goldstein, D.E. Ash, T.E. Elgren, D.M. Krutz, J.E. Penner-Hahn, Biochemistry 36 (1997) 9847.
[88] C.R. Natoli, Springer Series in Chemical Physics, vol. 27, Springer-Verlag, Berlin, 1983, p. 43.
[89] L.-S. Kau, D.J. Spira-Solomon, J.E. Penner-Hahn, K.O. Hodgson, E.I. Solomon, J. Am. Chem. Soc. 109 (1987) 6433.
[90] J.E. Hahn, M.S. Co, D.J. Spira, K.O. Hodgson, E.I. Solomon, Biochem. Biophys. Res. Commun. 112 (1983) 737.
[91] K. Peariso, D.L. Huffman, J.E. Penner-Hahn, T.V. O'Halloran, J. Am. Chem. Soc. 125 (2003) 342.
[92] M. DiDonato, H.F. Hsu, S. Narindrasorasak, L. Que, B. Sarkar, Biochemistry 39 (2000) 1890.
[93] M. Ralle, S. Lutsenko, N.J. Blackburn, J. Biol. Chem. 278 (2003) 23163.
[94] M. Ralle, M.J. Cooper, S. Lutsenko, N.J. Blackburn, J. Am. Chem. Soc. 120 (1998) 13525.
[95] T. Nittis, G.N. George, D.R. Winge, J. Biol. Chem. 276 (2001) 42520.
[96] R.A. Pufahl, C.P. Singer, K.L. Peariso, S.-J. Lin, P.J. Schmidt, C.J. Fahrni, V.C. Culotta, J.E. Penner-Hahn, T.V. O'Halloran, Science 278 (1997) 853.
[97] J.E. Penner-Hahn, Indian J. Chem. 41 (2002) 13.
[98] A.C. Rosenzweig, D.L. Huffman, M.Y. Hou, A.K. Wernimont, R.A. Pufahl, T.V. O'Halloran, Structure 7 (1999) 605.
[99] A. Changela, K. Chen, Y. Xue, J. Holschen, C.E. Outten, T.V. O'Halloran, A. Mondragon, Science 301 (2003) 1383.
[100] D.W.J. Cruickshank, Acta Crystallogr. Sect. D: Biol. Crystallogr. 55 (1999) 583.
[101] C.-C. Huang, P.J. Casey, C.A. Fierke, J. Biol. Chem. 272 (1997) 20.
[102] H.-W. Park, S.R. Boduluri, J.F. Moomaw, P.J. Casey, L.S. Beese, Science 275 (1997) 1800.
[103] Y. Reiss, M.S. Brown, J.L. Goldstein, J. Biol. Chem. 267 (1992) 6403.
[104] M.M. Harding, Acta Crystallogr. Sect. D: Biol. Crystallogr. 57 (2001) 401.
[105] K.C. Cheung, R.W. Strange, S.S. Hasnain, Acta Crystallogr. Sect. D: Biol. Crystallogr. 56 (2000) 697.
[106] N. Binsted, R.W. Strange, S.S. Hasnain, Biochemistry 31 (1992) 12117.
[107] A.J. Dent, Top. Catal. 18 (2002) 27.
[108] M.A. Newton, D.G. Burnaby, A.J. Dent, S. Diaz-Moreno, J. Evans, S.G. Fiddy, T. Neisius, S. Turin, J. Phys. Chem. B 106 (2002) 4214.
[109] M. Richwin, R. Zaeper, D. Lutzenkirchen-Hecht, R. Frahm, Rev. Sci. Instrum. 73 (2002) 1668.
[110] M. Haumann, M. Grabolle, T. Neisius, H. Dau, FEBS Lett. 512 (2002) 116.
[111] P.J. Riggs-Gelasco, L. Shu, S. Chen, D. Burdi, B.H. Huynh, L. Que Jr., J. Stubbe, J. Am. Chem. Soc. 120 (1998) 849.
[112] O. Kleifeld, A. Frenkel, J.M.L. Martin, I. Sagi, Nat. Struct. Biol. 10 (2003) 98.
[113] A. Frenkel, O. Kleifeld, S.R. Wasserman, I. Sagi, J. Chem. Phys. 116 (2002) 9449.
[114] T. Ressler, O. Timpe, T. Neisius, J. Find, G. Mestl, M. Dieterle, R. Schlogl, J. Catal. 191 (2000) 75.
[115] H. Rumpf, J. Janssen, H. Modrow, K. Winkler, J. Hormes, J. Solid State Chem. 163 (2002) 158.
[116] S.R. Wasserman, J. Phys. IV 7 (1997) 203.
[117] S.R. Wasserman, P.G. Allen, D.K. Shuh, J.J. Bucher, N.M. Edelstein, J. Synchrot. Radiat. 6 (1999) 284.
[118] G.W. Coulston, S.R. Bare, H. Kung, K. Birkeland, G.K. Bethke, R. Harlow, N. Herron, P.L. Lee, Science 275 (1997) 191.
[119] K. Zhang, J. Dong, D.S. Auld, Physica B 209 (1995) 719.
[120] D.S. Auld, K. Geoghegan, A. Galdes, B.L. Vallee, Biochemistry 25 (1986) 5156.
[121] M.R. Chance, M.D. Wirt, E.M. Scheuring, L.M. Miller, A.H. Xie, D.E. Sidelinger, Rev. Sci. Instrum. 64 (1993) 2035.

[122] J. Gailer, G.N. George, I.J. Pickering, S. Madden, R.C. Prince, E.Y. Yu, M.B. Denton, H.S. Younis, H.V. Aposhian, Chem. Res. Toxicol. 13 (2000) 1135.
[123] L.A. Polette, J.L. Gardea-Torresdey, R.R. Chianelli, G.N. George, I.J. Pickering, J. Arenas, Microchem. J. 65 (2000) 227.
[124] D.E. Salt, R.C. Prince, I.J. Pickering, Microchem. J. 71 (2002) 255.
[125] D.S. Auld, K.H. Falchuk, K. Zhang, M. Montorzi, B.L. Vallee, Proc. Natl. Acad. Sci. U.S.A. 93 (1996) 3227.
[126] C.T. Dillon, P.A. Lay, M. Cholewa, G.J.F. Legge, A.M. Bonin, T.J. Collins, K.L. Kostka, G. SheaMcCarthy, Chem. Res. Toxicol. 10 (1997) 533.
[127] W. Yun, S.T. Pratt, R.M. Miller, Z. Cai, D.B. Hunter, A.G. Jarstfer, K.M. Kemner, B. Lai, H.R. Lee, D.G. Legnini, W. Rodrigues, C.I. Smith, J. Synchrot. Radiat. 5 (1998) 1390.
[128] S. Yoshida, A. Ektessabi, S. Fujisawa, J. Synchrot. Radiat. 8 (2001) 998.
[129] M.D. Hall, C.T. Dillon, M. Zhang, P. Beale, Z. Cai, B. Lai, A.P.J. Stamp, T.W. Hambley, J. Biol. Inorg. Chem. 8 (2003) 726.
[130] C.G. Schroer, M. Kuhlmann, T.F. Gunzler, B. Lengeler, M. Richwin, B. Griesebock, D. Lutzenkirchen-Hecht, R. Frahm, E. Ziegler, A. Mashayekhi, D.R. Haeffner, J.D. Grunwaldt, A. Baiker, Appl.Phys. Lett. 82 (2003) 3360.